CHAPTER 3.

RUNOFF AND SEDIMENT YIELDS FROM AN UNPAVED ROAD SEGMENT, ST. JOHN, U.S. VIRGIN ISLANDS

ABSTRACT

Unpaved roads have been identified as the primary source of terrigenous sediments being delivered to marine ecosystems around the island of St. John. These sediments pose a threat to the growth and overall condition of nearshore coral reef communities. The goal of this project was to calibrate and test event-based runoff and sediment yield models for an unpaved road segment, as these could provide a better understanding of processes and help in the design of erosion control strategies. The specific objectives were to: (1) measure runoff and suspended sediment yields from a road segment; (2) develop, calibrate, and test the performance of two event-based runoff models; and (3) compare predicted suspended sediment yields to sediment yields measured by a sediment trap. The first runoff model (GA-UH) combines the Green-Ampt infiltration equation with an empirically-derived unit hydrograph. The second model (GA-KW) uses the same infiltration equation, but routes the excess precipitation using a physically-based kinematic wave approach.

Precipitation and runoff data were collected from a 230-m long, mostly-unpaved road segment in the Maho Bay area of St. John over an 8-month period. Over the study period there were 135 storm events with a total rainfall of 42.3 cm. Total runoff was of 9.8 cm from 26 events. From 0.3 to 0.5 cm of precipitation was needed to initiate runoff and discharge was non-linearly correlated with precipitation.

The two models were calibrated based on a set of eight storms. Both models performed very similarly when tested using a different set of 18 storm events. Model performance was poor for rainfall events smaller than 1 cm, but improved for larger events. These problems appear to be due to the difficulty of accurately characterizing infiltration rates during the initial portion of storm events. Overall, the GA-KW performed slightly better as it resulted in hydrographs with higher correlation values than those from GA-UH.

Suspended sediment concentration showed a significant non-linear correlation with runoff rates. Coupling the GA-KW model with an empirical sediment-rating curve estimated sediment yields that were linearly correlated with total precipitation ($r^2 = 0.93$). The estimated sediment yield rate of 0.29 kg m^{-2} per centimeter of precipitation was very similar to that measured by a sediment trap. However, yield rates by particle size categories showed that close agreement only occurred for sand-size particles, while large discrepancies existed for all other size categories. An erosion rate of 0.42 kg m^{-2} cm^{-1} (48 kg m^{-2} yr^{-1}) appears to be a more accurate sediment yield rate estimate for this road segment with eroded material consisting of 29% gravel, 31% sand, 38% silt, and 2% clay. The estimated annual sediment yield rate represents a four-order increase over rates measured from undisturbed hillslopes. The models developed by this study could be used as a tool to develop and implement better road drainage design aimed at reducing road erosion and sediment yields into the nearshore marine ecosystem of St. John.

3.1 Introduction

3.1.1 Problem Statement

Roads alter a series of processes that control the storage and distribution of water on the landscape. The most obvious effect of roads is to increase the frequency and magnitude of surface runoff by creating a compacted, low-permeability surface (Bren and Leitch, 1985; Harden, 1992; Ziegler and Giambelluca, 1997). Roads can intercept subsurface flows (e.g., Megahan, 1972) and disrupt natural drainage patterns (Montgomery, 1994). It is less clear whether these total changes can induce significant changes in runoff at the basin scale (Jones and Grant, 1996; Thomas and Megahan, 1998; La Marche and Lettenmaier, 2001).

Roads also alter the rate at which sediment is produced, routed, and eventually exported from a catchment. Surface erosion rates are typically much higher on cutslopes, fillslopes, and unpaved travelways than on undisturbed hillslopes (e.g., Megahan, 1978; Reid, 1981; Megahan et al., 2001). Hillslope gullies formed by the concentration of road drainage are an additional source of sediment and an important conduit for delivering runoff and sediment to the fluvial network (Wemple et al., 1996; Croke and Mockler, 2001). Unpaved roads have been shown to increase the frequency of mass-wasting events (e.g., Gresswell et al., 1979; Wemple et al., 2001) and watershed-scale sediment yields (e.g., Rice et al., 1979; Anderson and Potts, 1987).

The generation and delivery of terrestrial sediments is a particular concern in the eastern Caribbean because this can adversely affect nearshore coral reef communities (Hubbard, 1987). This issue has received special attention on the island of St. John because of the importance of the surrounding coral reefs to tourism and the local economy. Over 70 km^2 of St. John's offshore waters have been designated as an International Biosphere Reserve and are either part of the Virgin Islands National Park (VINP) or the V.I .Coral Reef National Monument.

Earlier studies showed that unpaved roads on St. John can increase sediment production rates at the plot and hillslope scale by several orders of magnitude relative to undisturbed areas (MacDonald et al., 2001). Unpaved roads are believed to be the primary source of fine sediment

being delivered to the marine environment (MacDonald et al., 1997; Anderson and MacDonald, 1998; Ramos-Scharrón and MacDonald, 2003). An empirical model developed from sediment trap data concluded that road erosion is a function of total precipitation, road gradient, drainage pattern, and the frequency of grading (Chapter 2). MacDonald et al. (2001) captured the runoff from several road segments and showed that only 6 mm of precipitation was needed to initiate overland flow but just 2 to 13% of the rainfall from small-to-moderate storms was transformed into runoff.

The primary limitation of earlier work was that it aggregated runoff and sediment yields from one or more storms. A more process-based understanding of the relationships between rainfall intensity, runoff rates, and suspended sediment concentrations is needed to better predict runoff and sediment yield at the road-segment scale. More process-based models could compensate for the likely underestimate of silt and clays from the sediment traps that have been used to assess sediment production rates on St. John (Sampson, 1999; Chapter 2; Chapter 4). More explicit models could also provide better predictions of runoff and erosion rates from more extreme events and make predictions for a wider range of road conditions.

The main objectives of this study were to: (1) assess the relationship between precipitation, runoff, and suspended sediment yields for a single road segment at a high temporal resolution; (2) develop, calibrate, and test the performance of two runoff models; (3) couple a runoff model with a sediment-rating curve; and (4) compare predicted sediment yields to values measured with a sediment trap and values estimated with an empirical road segment erosion model.

3.1.2 Previous Road-Runoff Studies and Models

Event-based models for predicting road runoff and suspended sediment yields generally share a three-step structure. First, models quantify rainfall excess by determining the difference between rainfall intensity and infiltration rates. Empirical models generally have either applied an average infiltration rate to all events (e.g., Reid, 1981) or constructed a time-dependent

infiltration capacity curve (e.g., Ziegler and Giambelluca, 1997). Runoff data from road plots also have been used to calibrate physically-based infiltration models (e.g., Luce, 1990; Ziegler et al. 2001a). Reported infiltration rates for unpaved roads range from 0.02 to 3.7 cm hr^{-1}, while calibrated or measured saturated hydraulic conductivity values have varied from 0.02 to 0.60 cm hr^{-1} (Table 1).

The second step in event-based modeling is to transform excess precipitation into an outflow hydrograph. Unit hydrographs have been a common method to transform excess precipitation into outflow (e.g., Kahklen, 1994; Reid and Dunne, 1984). More physically-based models for routing excess precipitation generally use a kinematic wave approach, where overland flow rates are approximated either by the Darcy-Weisbach (e.g., Luce and Cundy, 1992; Simons et al., 1977, 1978) or Manning's equations (e.g., Ziegler et al., 2001a).

The third component uses the predicted runoff to calculate sediment production rates. Some studies have used a sediment-rating curve, which is an empirical relationship between discharge and suspended sediment concentrations (e.g., Reid and Dunne, 1984). Alternatively, sediment production rates can be estimated by physically-based models. These compare the erosive forces applied by rainfall and overland flow to the erodibility of the road surface material (e.g., Simons et al., 1977, 1978). While erodibility is typically treated as a constant for a given road segment, the erodibility of a road surface can vary with maintenance practices, traffic, and the amount of material already eroded (Ziegler et al., 2000). At least one recent study has attempted to incorporate these effects into a more physically-based road erosion model (Ziegler et al., 2001a).

This study developed, calibrated, and tested the performance of two runoff models. The first model calculated infiltration rates using the Green-Ampt equation (GA). The precipitation excess estimated by this model (GA-UH) was transformed into outflow based on an empirically-derived unit hydrograph. The second model (GA-KW) also used the GA equation and combined

it with a kinematic wave routing approach. The GA-KW model was coupled with an empirical sediment rating curve to estimate sediment yields.

3.2 Study Area

St. John lies approximately 80 km east of Puerto Rico and is the third largest island of the U.S. Virgin Islands. The topography of St. John is very rugged, as more than 80% of the island has slopes greater than 30% (CH2M Hill, 1979; Anderson, 1994). Vegetation is dominated by dry evergreen formations and moist tropical forests (Woodburry and Weaver, 1987).

The climate of St. John is characterized as dry tropical. Easterly waves moving through the Caribbean are important contributors to rainfall from May through November, while cold fronts control the rainfall regime the rest of the year (Calversbert, 1970). Bowden et al. (1970) identified five different precipitation zones with values ranging from 89-102 cm yr^{-1} to 127-140 cm yr^{-1}. Precipitation in St. John can be highly erosive. Maximum 15-min intensities at Caneel Bay exceeded 10 cm hr^{-1} sixteen times between 1979 and 1995, and these were generally associated with the largest storm events. Sampson (1999) estimated that annual precipitation energy at Caneel Bay averages 13,500 MJ mm ha^{-1} hr^{-1}.

Rapid development on privately-owned lands has led to a dense network of unpaved roads. Construction and maintenance standards of public roads and private driveways are generally very poor. The spacing of effective road drainage structures (i.e., ditches, culverts, or cross-drains) is very sparse, even on extremely steep road segments. The steep gradients, poor drainage design, and high rainfall erosivity result in the development of deep rills on the road surfaces. Roads with considerable light vehicle traffic have to be regraded approximately every year.

Rainfall, runoff, and suspended sediment yields were collected from a 230-m long road segment in the Maho Bay area on the north-central portion of St. John (Figures 1 and 2a). The study segment (hereafter referred as Maho-Road) was divided into four sub-segments according to differences in road surface material and slope (Table 2). Maho-Road has a total road tread area

of 1,240 m^2, an average slope of 12.5%, and a partially-paved section that is 48 m long and has an area of 190 m^2. The partially-paved section has a thin layer of non-reinforced concrete on a poorly-prepared native surface. The concrete is breaking apart and exposes some of the underlying material. The unpaved portions of Maho-Road are regraded about twice a year, as deep rills on the road surface hinders the daily traffic load of 100-270 light vehicles and 4-6 heavy trucks.

Rocks in the Maho Bay area are part of the Picara Member of the Tutu Formation, which consist of metamorphosed volcanic wacke, conglomerate, siltstone, limestone, with some basalt (Rankin, 2002). Soils in the area are part of the Maho Bay loamy soil series (NRCS, 1995). These soils are typically shallow, moderately permeable, well drained, and underlain by nearly impervious material. These characteristics are largely responsible for the high infiltration rates on undisturbed areas and a lack of Hortonian overland flow. The average annual rainfall in the Maho Bay area is between 114 and 127 cm (Bowden et al., 1970).

3.3 Methods

3.3.1 Field Methods

Precipitation intensities were measured by rain gauges located about 25 m from the top or western end of Maho-Road (Figure 1). A weighing-bucket rain gauge provided one-hour precipitation intensity data with a resolution of 2.5 mm from 22 August 1999 to 2 September 1999, while a tipping-bucket rain gauge with a resolution of 0.25 mm was used from 2 September 1999 to 16 May 2000. The data collected by the tipping-bucket gauge were aggregated to 5-minute intervals. Individual storms were defined as a precipitation event separated from other events by at least one hour with no precipitation.

A 20.3-cm portable cutthroat flume was used to measure runoff (Figure 2b). The flume was installed in a natural swale about 8 m downslope from a broad dip that diverted all of the runoff from the road surface (Figure 1). The flume had a maximum capacity of 65 L s^{-1}, which

equates to a runoff rate of 19.0 cm hr^{-1} for the surface area of Maho-Road. Stage was measured at 5-minute intervals by a pressure transducer inserted into a stilling well attached to the flume, and recorded by a data logger. An equation provided by the flume manufacturer (Baski, Inc.) was used to convert the stage data to discharge. During some runoff events manual staff gage readings were taken at 2.5 to 5 minute intervals.

Data collection was interrupted several times during the study period. From 13 to 23 October 1999 the orifice leading to the stilling well was clogged with sediment, and this led to erroneous stage values. On 25 October 1999 the flume was dislodged by high flows and it was not reset until 30 October 1999. The flume was also dislodged on 17 November 1999 by runoff from Hurricane Lenny, and measurements were not resumed until 17 December 1999.

Since the road segment was unbounded and the flume was in a natural drainage, visual observations were used to identify when there was additional runoff from upslope areas. Observations during most of the storm events indicated that upslope areas produced runoff only during intense rainfall events with wet antecedent conditions. Subsurface flow interception at the road cutslopes was short-lived and very rare. Flow from upslope areas or the cutslope were observed on 12 November 1999, 17 November 1999, and 23 February 2000, and these events have been excluded from the data set.

During some flow events 1-6 grab samples were collected at the outlet of the flume in 250-ml plastic bottles. The samples were collected by submerging a bottle with a loosely-fitted cap into the flow, briefly removing the cap until the bottle was filled, and then replacing the cap before removing the bottle.

3.3.2 Modeling Infiltration Capacity

Direct calculation of an infiltration curve over time was not possible for time periods shorter than the duration of events because the infiltration losses could not be separated from the effects of flow routing along the road segment. The average infiltration rate for the road segment

was calculated for each event by subtracting the depth of runoff from precipitation, and dividing this value by the duration of runoff. By fitting a non-linear regression equation to the relationship between average infiltration rate and flow duration, infiltration rates could be estimated for 1-minute intervals (equation 1):

$$i(t_i) = \left[n \cdot \left\{\bar{I}(t_i)\right\}\right] - \sum_{1}^{i-1} i(t_i) \qquad \text{(eq. 1)}$$

where $i(t_i)$ is the infiltration *i* minutes after the beginning of the event, n is the rank of one-minute intervals with n=1 at five minutes after the onset of precipitation, $\bar{I}(t_i)$ is the average infiltration rate calculated from the regression equation on the relationship between average infiltration and duration, and $\sum_{1}^{i-1} i(t_i)$ is the summed infiltration from all previous time periods. The resulting infiltration rates were used to help select the initial values and limits for parameters in the Green-Ampt infiltration equation.

The Green-Ampt (GA) infiltration model is based on a one-dimensional approximation of Darcy's Law. It effectively assumes that piston flow creates a distinct wetting front, and that the suction head and hydraulic conductivity values are constant for a site (Scott, 2000). The GA model is:

$$i(t) = K_s\left[\frac{h_o + h_f + z_f(t)}{z_f(t)}\right] \qquad \text{(eq. 2)}$$

where i(t) is infiltration capacity in cm hr^{-1}, K_s is the saturated hydraulic conductivity in cm hr^{-1}, h_o is the depth of water ponded on the soil surface in centimeters, h_f is the suction head in centimeters, and $z_f(t)$ is the time-dependent depth of the wetting front in centimeters. As in previous studies, h_o was assumed to be zero to simplify calculations (e.g., Simons et al., 1977;

Flerchinger and Watts, 1987). By assuming that infiltrated water moves downwards as piston flow, the time-dependent depth of the wetting front can be estimated by:

$$z_f(t) = \frac{I(t)}{\Delta\theta_v} \quad \text{(eq. 3)}$$

where I(t) is the cumulative depth of infiltration in centimeters and $\Delta\theta_v$ is the volumetric water content deficit of the soil in $cm^3\ cm^{-3}$. The latter term is defined as the difference between the effective porosity of the soil, which is approximated by its water content at saturation (θ_{sat}), and the water content at the beginning of an individual storm event (θ_i). Combining equations 3 and 4, the infiltration rate can be expressed as:

$$i(t) = K_s\left[\frac{h_f \cdot \Delta\theta_v}{I(t)} + 1\right] \quad \text{(eq. 4)}$$

In the absence of data on changes in θ_v during and after storm events, it was not possible to directly model the increase in infiltration in periods without ponded water due to drying between storms. The initial values for K_s, h_f, and θ_{sat} were calibrated using only those storms with no 6-hr antecedent precipitation and an assumed value of zero for θ_i. θ_i was then used as the only calibration parameter for those events that had a 6-hr antecedent precipitation greater than zero.

Precipitation excess was calculated as the difference between precipitation intensities and the infiltration rates from equation 4. Precipitation excess was calculated using 2.5-minute time steps by assuming that the precipitation intensity for each 2.5-minute step was equal to those measured at a 5-minute resolution.

Three main differences exist in the use of the Green-Ampt infiltration equation by the GA-UH and the GA-KW models. First, the decline in infiltration over time was calculated in the GA-UH model every 5-minutes, while 2.5-minute time steps were used to calculate infiltration in

the GA-KW model. Second, water is available for infiltration in the GA-UH model only during the time step when it is being received as precipitation. All of the excess precipitation calculated by the GA-UH model is routed as overland flow to the outlet of Maho-Road by the unit hydrograph transform function. On the other hand, the GA-KW model continues to calculate infiltration losses even after precipitation has ceased. Total infiltration losses at times with no precipitation are further reduced by a scaling parameter. This parameter reduces the proportion of the Maho-Road with ponded water as the runoff successively drains from each of the four sub-segments. The value of this parameter is derived from an estimated average flow velocity and the length of each sub-segment.

The third difference between the two models with respect to the GA equation is that at each time step the GA-UH model calculates precipitation excess for the entire Maho-Road, while the GA-KW model calculates precipitation excess in each of the four sub-segments. In the GA-KW model the suction head, initial water content, and saturated water content are treated as lumped parameters, but the hydraulic conductivity has different values in the partially-paved and the unpaved sections. The lumped hydraulic conductivity value for Maho-Road ($K_{s\ road}$) used by the GA-UH model is defined in terms of the saturated hydraulic conductivity of both the partially-paved (K_p) and unpaved (K_u) road sections (Equation 5):

$$K_{s\ road} = \left[\frac{A_1 \cdot K_u}{A_t}\right] + \left[\frac{A_2 \cdot K_p}{A_t}\right] + \left[\frac{A_3 \cdot K_u}{A_t}\right] + \left[\frac{A_4 \cdot K_u}{A_t}\right] \qquad \text{(eq. 5)}$$

where $K_{s\ road}$ is in cm hr^{-1}, A_i is the area in m^2 for each of the four road sub-segments, A_t is the total road segment area in m^2, and K_u and K_p are in cm hr^{-1}.

3.3.3 Unit Hydrograph Runoff Modeling

The unit hydrograph (UH) is an empirically-defined function that transforms precipitation excess into an outflow hydrograph (McCuen, 1998). The UH approach assumes that the runoff

hydrograph is linearly proportional to excess precipitation, and that the duration of the runoff hydrograph is constant for storms with the same duration (Gray, 1960). Hydrographs from eight storms were used to develop a 2.5-minute unit hydrograph following the rainfall-excess reciprocal method (Dunne and Leopold, 1978). These events were selected because the method requires hydrographs that are single-peaked and generated by storms with similar durations. These criteria meant that the eight storms used were all short-duration and had generally low runoff rates (Appendix II-A).

Runoff data with a 2.5-min resolution were available for all eight of these storms except for the 27 September-c 1999 and 4 January 2000 events, which had data at a 5-minute resolution. The S-Hydrograph method was used to transform the 5-minute unit hydrographs derived from these two storms into 2.5-minute unit hydrographs (McCuen, 1998). The eight 2.5-minute unit hydrographs were shifted in time so that their origin was set at the same time relative to the beginning of excess rainfall (Appendix II-A). The final unit hydrograph was constructed by calculating the mean flow value for each 2.5-minute interval. No additional normalization was required as the resulting unit hydrograph represented one centimeter of precipitation excess.

3.3.4 Kinematic Wave Runoff Modeling

Kinematic waves are a simplified version of the one-dimensional, distributed routing models described by the St. Venant equations (Chow, 1998). These equations include the effect of momentum while neglecting the dynamic effects of pressure and acceleration. Hence the movement of water over a plane can be defined by any equation that conserves momentum, such as Manning's equation (equation 6). The transfer of water from one plane to another can be described by mass conservation (equation 7).

$$Q = \left[\frac{S_o^{1/2}}{n \cdot P^{2/3}} \right] \cdot A \qquad \text{(eq. 6)}$$

$$q = \frac{\delta Q}{\delta x} + \frac{\delta A}{\delta t} \quad \text{(eq. 7)}$$

In these equations Q is discharge in $m^3\ s^{-1}$, S_o represents the downstream water surface slope in percent, n is Manning's roughness coefficient in seconds $m^{-1/3}$, P is the wetted perimeter of the flow in meters, A is the flow area in m^2, x is downslope distance in meters, t is time in seconds, and q refers to inflows or outflows in $m^3\ s^{-1}$ in the form of precipitation or infiltration. A can be expressed as a power function of Q (equation 8):

$$A = \alpha Q^{\beta} \quad \text{(eq. 8)}$$

where α and β are empirical coefficients. Equations 6 and 8 can be combined to calculate α, while β is usually set to 0.60 (Chow, 1998). After differentiating by time, equation 8 can be combined with equation 7 to produce the kinematic flow equation (equation 9):

$$q = \frac{\delta Q}{\delta x} + \left[\alpha \beta Q^{\beta-1} \left(\frac{\delta Q}{\delta t} \right) \right] \quad \text{(eq. 9)}$$

Since discharge (Q) is the only dependent variable, all of other parameters can be measured or estimated from the physical characteristics of the overland flow plane.

Equation 9 was solved for the Maho-Road by following a backward linear difference method to approximate the time and space derivative of discharge (Chow, 1998). The solution to equation 9 was used to calculate the discharge from each of the four sub-segments.

One difficulty of the kinematic wave approach is that discharge on the recession limb asymptotically approaches zero (Henderson and Wooding, 1964). This results in infinitely long recession limbs, which do not match field observations. This problem was noted in the GA-KW simulations and stems from the lack of infiltration during the latter stages of the runoff hydrograph when the scaling parameter had reduced the proportion of the road still experiencing

infiltration to zero. This problem was solved by forcing all flows less than 0.03 cm hr^{-1} to zero, as this discharge is lower than the minimum flow that could be measured with the flume.

3.3.5 Model Calibration

Model calibration required the simultaneous consideration of different parameters. The GA equation has four input parameters that require calibration (K_s, h_f, θ_i, and θ_{sat}). The GA-UH model did not require calibration of parameters in addition to those needed by the GA equation, but additional calibration parameters in the GA-KW model were the hydraulic conductivity (K_s) and surface roughness (n) values for each of the sub-segments.

The calibration of both routing methods was done manually using a multi-objective calibration procedure. The three objectives used for calibration and assessing model error were the percent error in total discharge, the coefficient of determination (R^2) for the overall shapes of the simulated hydrographs as defined by Nash and Sutcliffe (1970), and the percent error in peak discharge. The coefficient of determination is defined as:

$$R^2 = \frac{\sum (q_i - \overline{q}_i)^2 - \sum (\hat{q}_i - q_i)^2}{\sum (q_i - \overline{q}_i)^2} \qquad \text{(eq. 10)}$$

where q_i is the measured discharge at time i, $\overline{q}_i$ is the mean of all measured runoff rates, and $\hat{q}_i$ is the predicted runoff at time i. An R^2 value of 1.0 indicates perfect agreement, while a negative value indicates that the error in the predicted hydrograph is greater than the variability of the observed hydrograph around the mean discharge. Both routing models were calibrated using the same eight storms used to develop the unit hydrograph.

3.3.6 Suspended Sediment Analysis and Modeling

A total of 70 suspended sediment samples were collected during 21 storm events over the 8-month study period. Suspended sediment concentrations were determined by measuring the

volume of the sample, filtering it using a pre-weighed 24-cm diameter ashless filter with a pore size of 3 μm, drying the filter at 100-110º C for about 24 hours, and weighing it to the nearest 0.01 g. Forty-six samples were also analyzed for their particle-size distribution by use of the hydrometer method (Gee and Bauder, 1986). Regression analyses were used to determine whether discharge affected either the suspended sediment concentration or the particle-size distribution.

3.3.7 Model Application

The GA-UH and GA-KW models were used to estimate total runoff for the 160 storms larger than 0.07 cm that occurred between 2 September 1999 and 19 May 2000. Total discharge predicted for these 160 events was used to estimate runoff responses for storms with precipitation exceeding 2.8 cm, which was the size of the largest storm used for calibration and validation. The performances of the two models were compared on the basis of their percent error in total discharge, the coefficient of determination, and percent error in peak discharge.

Predicted hydrographs from the model with the best overall performance were combined with the empirical sediment-rating curve to estimate suspended sediment yields for all 160 storm events. The mean sediment yield per cm of rainfall value resulting from the runoff-sediment rating curve model was compared to that measured by a sediment trap and that estimated by a general road erosion model (Chapter 2).

3.4 Results

3.4.1 General Results

Reliable precipitation and runoff data were obtained for 135 events with a total rainfall of 41.3 cm between 2 September 1999 and 16 May 2000. These storms lasted for only 10-30 minutes. The largest storm had 2.8 cm of precipitation, a maximum 5-minute intensity of 12.8 cm hr^{-1}, and a total erosivity of 38.6 MJ cm ha^{-1} hr^{-1}.

Twenty-six of these 135 events produced runoff, and the total discharge was 9.8 cm or 24% of the total rainfall (Table 3). The mean rainfall of the 26 runoff-producing storms was 0.95 cm as opposed to 0.15 cm for the 109 events that did not generate runoff. Total discharge showed a non-linear increase with total rainfall (Figure 3). At least 0.3 to 0.5 cm of rainfall and a 5-minute intensity of 1.8 cm hr^{-1} were required to initiate runoff. Runoff coefficients for storms with less than 1.3 cm of precipitation ranged up to 0.61, while the runoff coefficients for storms larger than 2.2 cm ranged from 0.39 to 0.76 (Table 3; Appendix II-B). The highest peak discharge rate was 12.0 cm hr^{-1} from a storm with a maximum 5-minute rainfall intensity of 7.6 cm hr^{-1}. Peak flow rates were strongly correlated with total precipitation (r^2=0.81), and this is because the larger events tended to have higher precipitation intensities (Appendix II-B).

3.4.2 Infiltration Curve

The mean infiltration rate was 1.2 cm hr^{-1} for the 26 events that generated runoff, and the range was from 0.25 to 3.8 cm hr^{-1}. Average infiltration rates were initially highly variable but tended to approximate an asymptotic rate of 0.4 cm hr^{-1} after 40 minutes (Figure 4). The regression equation from Figure 4 was combined with equation 1 to calculate the infiltration curve for Maho-Road (Figure 5). The infiltration rate was limited to 4.0 cm hr^{-1} for the first 10 minutes of an event in order to eliminate the problem of infinitely high infiltration rates at very short time periods. This value is slightly higher than the maximum average infiltration rate in Figure 4. The resulting infiltration curve approaches an asymptotic value of 0.17 cm hr^{-1} by 30 minutes after the onset of infiltration (Figure 5). The estimated asymptotic value of 0.17 cm hr^{-1} was used as the initial estimate of the saturated hydraulic conductivity of the road surface in the GA model.

3.4.3 GA-UH Model Calibration

The mean 2.5-minute unit hydrograph for 1.0 cm of runoff is shown in Figure 6. This has a time to peak of 2.5 minutes, a peak runoff rate of 10.0 cm hr^{-1}, and a total duration of 37.5 minutes. Table 4 shows the range of values considered in calibrating the four parameters needed for the GA-UH model (Equation 4). The mean K_s for Maho-Road ranged only from 0.12 to 0.22 cm hr^{-1}, as this should remain close to the value of 0.17 cm hr^{-1} estimated from the infiltration curve (Figure 5). A value of 0.20 cm hr^{-1} yielded the best match to the observed hydrographs. This value is similar to the other values in the literature (Table 1).

Suction head was allowed to vary between 2.0 and 8.0 cm, as this was the range of values found by Flerchinger and Watts (1987) for unpaved roads in the western United States. A suction head of 5.4 cm was used for the GA-UH model.

The saturated water content (θ_{sat}) was allowed to vary between 0.25 and 0.60 cm^3 cm^{-3}. The low-end was similar to the minimum values found by Flerchinger and Watts (1987) for unpaved roads and the high-end was comparable to the value determined for sandy-loam soils (Rawls et al., 1983). This range also falls within the porosity values of 0.25 to 0.40 cm^3 cm^{-3} back-calculated from the surface bulk-density of unpaved roads (Helvey and Kochenderfer, 1990). A θ_{sat} of 0.40 cm^3 cm^{-3} provided the best calibration for the GA-UH model.

During the calibration procedure it was noted that storms with precipitation in the previous six hours necessitated lower infiltration rates than storms without antecedent rainfall. The effect of antecedent precipitation on infiltration was addressed by varying θ_i. A θ_i value of zero was assigned to storms with no 6-hr antecedent precipitation, while θ_i was set to 0.18 cm^3 cm^{-3} for storms with 6-hr antecedent precipitation.

3.4.4 GA-KW Model Calibration

The saturated hydraulic conductivity values for the unpaved (K_u) and paved sections (K_p) of Maho-Road were calculated by applying equation 5 to the different sub-segments listed in Table 2. $K_{s\ road}$ was set to 0.20 cm hr^{-1} in accordance with the results of the GA-UH model calibration, and this resulted in equation 11.

$$K_p = 1.10 - 5.49 * K_u \quad \text{(eq. 11)}$$

K_u values ranged from 0.17 to 0.20 cm hr^{-1} in order to keep K_p greater than zero, but lower than K_u. The final hydraulic conductivity values for the GA-KW model were 0.23 and 0.04 cm hr^{-1} for the unpaved and partially-paved sub-segments, respectively. The chosen K_u value falls within the range of values used in previous studies (Table 1).

The calibrated value of θ_{sat} in the GA-KW model was the same as for the GA-UH model (0.40 $cm^3\ cm^{-3}$) and the suction head was 6.4 cm, or only slightly higher than the 5.4 cm used in the GA-UH model. θ_i for storm events with no 6-hr antecedent precipitation was assumed to be zero, while a θ_i of 0.11 $cm^3\ cm^{-3}$ was used for events that had antecedent precipitation.

The typical duration of the recession limbs was about 22.5 minutes after the end of precipitation. This suggested that 22.5 minutes was needed for runoff to travel from the top of the road segment to its outlet. Given the total length of 230 m, this yields an average velocity of 0.17 m s^{-1} (10.3 m min^{-1}). Hence, the empirical scaling factor (S_c) to attenuate infiltration after the end of precipitation was defined as:

$$S_c = 1 - \left(t_0 \cdot \frac{10.3}{l_i} \right) \quad \text{(eq. 12)}$$

where t_0 is the time in minutes after the precipitation or inflow from upslope sections has ceased, and l_i is the length of road section *i* in meters (Table 2).

Manning's n for the unpaved sections was allowed to vary from 0.01 to 0.03 s $m^{-1/3}$ (Table 4). This range was based on values for bare sand and graveled surfaces (Woolhiser, 1975). Manning's n for the concrete paved section was varied from 0.010 to 0.013 s $m^{-1/3}$ (Woolhiser, 1975). A common value of 0.010 s $m^{-1/3}$ was finally chosen for both surfaces. Given the advanced state of decay of the concrete in the partially-paved sub-segment it seems reasonable to accept a common surface roughness value for the unpaved and partially-paved sub-segments.

3.4.5 Model Validation

3.4.5.1 GA-UH Model

The GA-UH model was used to compute hydrographs for the 18 events in Table 3 that were not used for calibration (Table 5; Appendix II-C). The mean observed runoff was 0.51 cm, the mean absolute error in the predicted runoff was 0.15 cm or 29%. Absolute errors for individual storms ranged up to 0.63 cm or 43%. Runoff coefficients ranged from 0.00 to 0.72 cm cm^{-1}. The mean runoff coefficient of the predictions was 0.32 cm cm^{-1} or only 10% lower than the observed value of 0.36 cm cm^{-1}.

The accuracy of the GA-UH model in predicting discharge increases with increasing discharge totals. The model predicted runoff for only two of the seven events with less than 0.7 cm of precipitation and exhibited no trends in the absolute error in discharge with increasing runoff (Figure 7). The mean absolute error for the fourteen events with less than 0.5 cm of runoff was 0.13 cm or 69%. The mean absolute error for the four storms exceeding 0.5 cm of discharge was 0.21 cm or 32%.

The overall agreement between observed and simulated hydrographs as expressed by the R^2 parameter was highly variable. The mean R^2 value for the GA-UH model was –0.06 (n=13 storms), with values ranging from –2.21 to 0.67. The events with the largest rainfall totals generally had the lowest variability and the highest R^2 values (Figure 8). R^2 values for the seven

storms with less than 1 cm of precipitation for which runoff was predicted was –0.59 (s.d. = 1.23), while storms larger than 1 cm had an average value of 0.57 (s.d. = 0.19).

The predicted peak flow timings were much closer to the observed values than the magnitude of peak flows. The mean error in the timing of the predicted peak flows was 1.7 minutes. The GA-UH model did tend to predict longer and less steep recession limbs than the observed hydrographs. The mean difference between the observed and predicted peak flows was 1.3 cm hr^{-1} or 61%, with individual values ranging from 0.05 to 5.8 cm hr^{-1} (Figure 8). The model tended to underestimate the largest peak flows and the predicted peak flows were within 25% of the observed value for only three of the 18 storms used for validation (Figure 9).

The rainfall, observed runoff, and predicted runoff for the 5 January 2000 and the 27 September-c 1999 events are shown in Figures 10a and 10b, respectively. Total precipitation in the first of these two storms was 2.36 cm, and the total runoff was within 9% of the measured value (Figure 10a). In Figure 10b the GA-UH model predicted 3.3 times more discharge than the observed and the R^2 value was -1.83. The GA-UH simulations presented in Figures 10a and 10b show two typical errors in predicted hydrographs. First, predicted hydrographs were more responsive to changes in precipitation than observed hydrographs. Second, simulated hydrographs had a tendency to have longer and less steep recession limbs than the observed.

3.4.5.2 GA-KW Model

The GA-KW model was used to predict runoff for the same 18 events that were used to evaluate the GA-UH model (Table 5; Appendix II-D). Mean observed runoff was 0.47 cm and the mean absolute error in the predicted runoff was 0.15 cm or 32%. Absolute errors for individual storms ranged from 0.01 to 0.52 cm. Runoff coefficients ranged from 0.00 to 0.68 cm cm^{-1}. The mean runoff coefficient was 0.26 cm cm^{-1} or 28% lower than the observed value of 0.36 cm cm^{-1}.

The GA-KW model was unable to accurately estimate runoff for the smallest storms, as it predicted no runoff for six of the seven events with less than 0.7 cm of precipitation. The ability of the model to match observed discharges increases with increasing storm size. There were no trends in the absolute error in predicted runoff with an increase in the observed discharge (Figure 7). The mean absolute error for events with less than 0.5 cm of runoff was 0.13 cm or 76%, while the mean error for those storms exceeding 0.5 cm of runoff was 0.23 cm or 31%. Overall, the GA-KW model estimated discharges that were slightly lower than those resulting from the GA-UH model.

The mean R^2 for the predicted hydrographs using the GA-KW model was 0.29 (n=12 storms). The largest events generally had the lowest variability in R^2 and the highest and most consistent R^2 values (Figure 8). The R^2 values for the six smallest storms with predicted runoff was -0.08 (s.d. = 0.75), while the mean R^2 for storms with more than 1.0 cm or precipitation was 0.67 (s.d. = 0.22). While the GA-UH and GA-KW models generally produced hydrographs with similar R^2 values, the GA-KW model resulted in hydrographs with higher correlation values than those resulting from GA-UH.

As in the case of the GA-UH model, the predicted peak flows generally were within 2.5 minutes of the observed peaks (Appendix II-D). The GA-KW model also tended to predict longer and less steep recession limbs than the observed hydrographs. The predicted peak flows were generally lower than the observed, especially for the events with the largest peak flows (Figure 9). The mean absolute difference between the observed and the predicted peak flows was 1.3 cm hr^{-1} or 61%, with individual values ranging from 0.05 to 5.3 cm hr^{-1}. Out of the eighteen storms used for model validation, the predicted peak flows were within 25% of the observed values for only two events. The GA-KW model predicted slightly higher peak runoff rates than the GA-UH model, especially for events with observed peak rates exceeding 3.7 cm hr^{-1}.

The GA-KW model produced a hydrograph that was very similar to the observed for the 5 January 2000 event (Figure 10a). The predicted hydrograph for this storm had a R^2 of 0.74 and

a total predicted discharge that was within 1% of the measured runoff. Figure 10b shows an event for which the model produced a hydrograph that did not agree as well with the observed, as evidenced by a R^2 value of –1.53 and a predicted total discharge that was 3.1 times higher than the observed. As in the case with the GA-UH model, these two examples demonstrate that hydrographs predicted by the GA-KW model also predicted hydrographs that were more responsive to changes in precipitation than the observed and recession limbs that were longer and less steep than those from measured hydrographs.

3.4.6 Suspended Sediment Concentration and Yields

The mean suspended sediment concentration for all 70 samples was 20,800 mg L^{-1} (s.d. 17,800 mg L^{-1}), and the range was from 1,270 to 84,400 mg L^{-1}. This range is consistent with values from other studies (Table 1).

Suspended sediment concentrations rapidly increased with discharge, but beyond approximately 0.5 cm hr^{-1} there was no clear relationship between discharge and suspended sediment concentrations (Figure 11). The highest concentrations were for 27 samples collected over eight storms between 12 September and 25 October 1999. The mean concentration during these storms was nearly 30,000 mg L^{-1} compared to 15,300 mg L^{-1} for the remaining 43 samples. These higher suspended sediment concentrations are presumed to be associated with an increase in erodibility caused by grading of the road surface on 10 September 1999.

Non-linear regression analysis of concentration as a function of discharge for samples that were presumably affected by grading resulted in an exponent equal to 0.25, and the exponent for samples not affected by grading was 0.20. The differences in the exponents for graded and ungraded samples were not significant. As a result the entire 70 samples were used to develop the following sediment-rating curve:

$$C_o = 26{,}500 \cdot Q^{0.233} \qquad \text{(eq. 13)}$$

where C_o is total suspended sediment concentration in mg L^{-1} and Q is the instantaneous runoff rate in cm hr^{-1}. The use of a single sediment rating curve assumes a constant relationship between discharge and suspended sediment concentration, and thereby implicitly assumes constant erodibility of the road surface.

The particle-size distribution was determined for 46 samples from 18 different storm events with discharge ranging from 0.03 to 14 cm hr^{-1}. The relative percentage of sand, silt, and clay was highly variable, and there was no correlation between discharge and the particle-size distribution. On average, the samples consisted of 40% sand, 56% silt, and 3% clay with standard deviations of 34%, 34%, and 11%, respectively.

An analysis of the particle-size distributions over time showed that the amount of sand tended to be highest in the six weeks immediately after grading (Appendix II-E). During this period the mean percent sand was 65% and the mean percent silt was 34%. Nine samples had sand contents exceeding 75%. For the other 27 samples the mean sand content was 22% and the mean silt content was 70%. Since this increase in sand content coincides with the increase in sediment concentrations, no changes in the concentration of silt or clay appear to have occurred as a response to the regrading operation (Appendix II-E).

3.4.7 Model Application

3.4.7.1 Runoff

Both models were used to estimate the runoff from all of the 160 storms between 2 September 1999 and 19 May 2000 with at least 0.07 cm of precipitation. Ninety percent of these events had less than 1.0 cm of rainfall, but these events represented only 49% of the total rainfall over this period (Figure 12). Only 10% of the storms had more than 1.0 cm of rainfall, but these accounted for 51% of the total rainfall. The largest event during this period had 9.4 cm of rainfall and a maximum 5-minute precipitation intensity of 11.3 cm hr^{-1}. Long-term precipitation data

from Caneel Bay confirm that storms with less than 1.0 cm of precipitation represent nearly 90% of all storms, but account for only 49% of the total rainfall.

The total runoff estimated by the GA-UH model was 6% higher than the GA-KW model. Both models show a transition from a non-linear relationship between discharge and precipitation to a more linear trend for events with higher precipitation totals than those used for calibration or validation (Appendix II-B). For the 144 events with less than 1.0 cm of precipitation, the predicted runoff from the GA-UH model was 3.6 cm or 67% larger than the comparable value using the GA-KW model. For the larger events the difference in total runoff was only 2.8 cm or 6%. Although both models produced similar results, the GA-KW model was used to estimate runoff and sediment yields because it yielded a better overall match to observed hydrographs.

The predicted runoff for five different storm size classes using the GA-KW model are shown in Figure 12. The storm events larger than 1.0 cm produce 92% of the estimated runoff. The two storms with more than 5 cm of rainfall produced 17% of the total rainfall and 40% of the total runoff.

3.4.7.2 Sediment Yield

The limited number of suspended sediment samples meant that the accuracy of predicted sediment yields could not be tested against measured data. Nevertheless, by coupling the GA-KW model with the sediment rating curve (equation 13), it is possible to estimate sediment yields for the same group of 160 storm events for which total runoff was calculated.

The predicted sediment yields for five different storm size classes are shown in Figure 12. This shows that the storm events larger than 1.0 cm produced 95% of the total sediment yield. The maximum sediment yield for a single storm was 3,900 kg for a 9.4-cm storm on 23 February 2000. The two storms with more than 5 cm of rainfall produced 17% of the total rainfall but 45% of the total sediment yield.

3.5 Discussion

3.5.1 Predicted Runoff

Comparisons of the observed and predicted hydrographs showed similar errors for both models. Both models underestimated the amount of runoff for storms with less than 1 cm of rainfall, underestimated peak flows, and overestimated flow duration. These errors appear to be related to the calculation of precipitation excess rather than to the routing of runoff. The fact that both models are experiencing the same problems, and that their routing algorithms seem to represent different flow velocities, was interpreted as an indication that the routing of runoff was playing a secondary role to the development of precipitation excess. The mean unit hydrograph was derived from relatively small events with low runoff rates, and thus relatively slow flow velocities (Julien, 1995). In contrast, calibrated Manning's n values for both the unpaved and paved sub-segments in the GA-KW model was only 0.010 s $m^{-1/3}$, which was the lowest calibration value allowed for these parameters (Table 4). This low Manning's n value allows relatively high flow velocities given the inverse relationship between flow velocity and Manning's n (Equation 6).

The measured hydrographs showed considerable variability in total discharge for the storms with less than 1 cm of precipitation (Figure 3). The 0.00 to 0.48 cm total discharges shown for these small storms are comparable to the 0.00 to 0.38 cm discharge range previously reported for storms smaller than 1 cm for other roads on St. John (Sampson, 1999; MacDonald et al., 2001). The observed variability in total discharge and the errors in estimating runoff hydrographs appear to result from large fluctuations in infiltration rates occurring at the beginning of different storm events.

At the beginning of a storm infiltration rates were estimated from the steep portion of the infiltration curve defined by the GA equation. Large errors in the estimation of precipitation excess were likely, given the large changes in infiltration rates during the initial 20 to 25 minutes of an event (Figure 5). Both models were generally unable to predict any discharge for storms

smaller than 0.7 cm and they produced hydrographs with attenuated peak flows relative to the observed. This suggests that the GA model consistently erred in its predictions of initial infiltration by estimating rates that were too high relative to infiltration rates in the field. The calibration procedure resulted in hydraulic conductivity values that appear to compensate for too little runoff during the beginning of an event by considerably decreasing infiltration rates during latter periods. The resulting hydrographs are more responsive to precipitation and longer than the observed.

Previous efforts to physically model road surface runoff at the plot scale also have had problems in accurately predicting discharge during the initial stages of storms. These problems have been attributed to difficulties in quantifying depression storage, as well as antecedent soil moisture content and infiltration rates during the initial stages of storm events (Simons et al., 1978; Luce, 1990; Luce and Cundy, 1994).

3.5.2 Estimated Sediment Yields

The suspended sediment yields estimated by coupling the GA-KW model with the sediment rating curve (equation 13) were compared to sediment trap data for Maho-Road and an empirical sediment production model at the road segment scale (Chapter 2) hereafter referred as the R&M model. The R&M model uses total precipitation, average road slope, and frequency of road grading to predict the mass of sediment collected in traps. Sediment production for a given road segment was found to be linearly related to total precipitation. This has been interpreted as an indication that runoff, precipitation, and suspended sediment yields are linearly correlated. Therefore, the interpretation implies that, in the absence of grading, the concentration of suspended sediment in road runoff must remain rather constant over a time period not exceeding two years. Roads that were graded within the last two years produced more sediment than road segments that had not been graded over two years, but the sediment trap data did not show a short-term increase in sediment production immediately after grading.

In contrast, the suspended sediment data from Maho-Road showed higher sediment concentrations for the first six weeks after grading. During this period there were 22 cm of rainfall and an estimated 6.6 cm of runoff, and this may have been enough runoff to remove much of the easily erodible material. It appears that peaks in sediment production immediately after grading are too short-lived to alter the longer-term sediment yields that were measured with the sediment traps.

Sediment yield rates were estimated by coupling the GA-KW model with the empirical sediment-rating curve (equation 13) for 160 storms between 2 September 1999 and 19 May 2000. The estimated sediment yield was linearly related to precipitation ($R^2 = 0.93$) (Figure 13). The predicted sediment yields from the GA-KW-sediment rating curve model closely match the sediment trap data while the estimated sediment yields using the GA-KW-sediment rating curve are 50% higher than the values predicted by the R&M model.

The apparent similarity in sediment yield rates between the GA-KW-sediment rating curve model, the sediment trap data, and the R&M model does not verify these models, as the three values represent very different particle-size distributions. The mean particle-size distribution for the suspended sediment samples was much finer than the mass-weighted size distribution of the material collected from the sediment trap (Figure 14). The median particle size (D_{50}) for the suspended sediment samples was 0.02 mm versus 0.5 mm for the sediment trap data. The suspended sediment samples did not contain any material larger than coarse sand, while the material captured in the sediment trap consisted of 42% gravel, 51% sand, 5% silt, and 2% clay. The estimated production rates for silt from the GA-KW-sediment rating curve model were 9 times higher than the sediment trap.

The discrepancy in sediment production rates by particle-size class can be attributed to the differences in how sediment production was measured. Grab samples are unlikely to collect gravel-sized fragments for two reasons. First, the transport of coarse fragments is intermittent and spatially-variable across the bottom of the flume. Given the small volume of the sample

bottles, the collection of these particles is unlikely. Second, the coarser particles were probably produced during the most intense storm events when samples were not collected. In contrast, sediment traps are most effective in trapping larger particles but they are less effective in trapping particles finer than 0.025 mm (Ice, 1986).

The actual sediment production rate from Maho-Road is probably closer to 0.42 kg m^2 per centimeter of precipitation than the 0.29 or 0.27 kg m^{-2} cm^{-1} estimated by the GA-KW-sediment rating curve model and sediment trap, respectively. This estimate is obtained by summing the estimated silt and clay fractions from the suspended sediment data to the sand and gravel fraction from the sediment trap. This yields an average of 27% gravel, 33% sand, 38% silt, and 2% clay.

The particle-size distribution of material produced from unpaved road surfaces may vary widely among different sites. The variability is a result of differences in rainfall erosivities, overland flow erosive forces, and road surface particle-size distributions. Only a few studies have measured the entire size distribution of sediment eroded from road segments—including both its suspended and bed load components (Table 1). In New Zealand the sediment from unpaved roads in areas dominated by silty clays and silty-clay loams was 85% silt and clay and only 15% sand or coarser material (Fahey and Coker, 1992). In Australia about two-thirds of the annual sediment production from roads was transported as suspended sediment (Grayson et al., 1993). These contrast with the 40% of silt and clay-sized material being produced from the Maho-Road in St. John.

Results presented here show that unpaved roads in St. John can produce sediment at a very high rate. Assuming an annual rainfall rate of 115 cm, the Maho-Road is estimated to erode at a rate of nearly 50 kg m^{-2} yr^{-1}. This rate is four orders of magnitude higher than for undisturbed zero-order hillslopes (Chapter 4). This confirms the important role of unpaved roads in producing sediment on St. John. The event-based models developed by this study may improve runoff and sediment yield predictions for unpaved roads on St. John. Better predictions may

result in the improvement of road drainage design, and a reduction on the quantity of sediment reaching the marine environment of St. John.

3.6 Conclusions

Precipitation and runoff data were collected from 135 storms on a 230-m long road segment on the island of St. John. These storms produced 41.3 cm of rainfall, and the precipitation for individual storms ranged up to 2.84 cm. Five-minute rainfall intensities ranged up to 12 cm hr^{-1}. Only 9.8 cm or 24% of this precipitation was converted into runoff. Between 0.3 and 0.5 cm of precipitation were needed to initiate runoff and only 26 of the 135 storms generated runoff. Runoff increased non-linearly with storm rainfall ($p < 0.0001$). The calculated mean infiltration rate for the 26 events that produced runoff was 1.2 cm hr^{-1}, and the range was from 0.25 to 3.8 cm hr^{-1}. Average infiltration rates were initially highly variable but tended to approximate an asymptotic rate of 0.4 cm hr^{-1} after 40 minutes.

Precipitation and runoff data from eight events were used to develop and calibrate two runoff models. The first model (GA-UH) predicted runoff using the Green-Ampt infiltration equation and an empirically-derived unit hydrograph. The second model (GA-KW) used the Green-Ampt infiltration equation to calculate precipitation excess and a kinematic wave approach to route this runoff. Model calibration yielded parameter sets with physically realistic values.

The two models were evaluated by comparing predicted against measured hydrographs for the other 18 storms. The GA-UH model had a mean error in discharge prediction of 29%, a mean absolute difference between predicted and observed peak flows of 1.3 cm hr^{-1}, and a mean R^2 of –0.06. The GA-KW model had a mean error in discharge prediction of 32%, a mean absolute difference between predicted and observed peak flows of 1.3 cm hr^{-1}, and a mean R^2 value of 0.29. The predicted hydrographs from the two models were very similar, as both models predicted no runoff for most events with less than 0.7 cm of rainfall. Errors in predicting discharge did not increase with increasing storm size. Both models tended to underestimate peak

flows. Much of the error in predicting storm runoff was attributed to the difficulty of predicting the initial infiltration rate. Overall, the GA-KW model performed slightly better than the GA-UH model.

The mean suspended sediment concentration from 70 grab samples was 20,800 mg L^{-1}, and the maximum values were around 84,400 mg L^{-1}. Suspended sediment concentrations increased non-linearly with discharge ($p < 0.0001$). Grading appeared to increase sediment concentrations for approximately six weeks. By combining the GA-KW model with the sediment rating curve, the sediment yield for 160 storm events was 0.29 kg m^{-2} per centimeter of rainfall. This value was very similar to the value of 0.27 kg m^{-2} cm^{-1} determined from sediment trap data for the same road segment.

The similarity between these erosion rates does not verify either value as the modeled sediment yield was dominated by fine particles and the sediment trap captured mostly sand and gravel. There was close agreement only for the sand-sized particles. Given the sampling bias of each method, the true sediment yield can be more accurately estimated by summing the rates for silt and clay from the models developed here to the sand and gravel material measured from the sediment fence. On this basis the total sediment yield for the road segment is estimated to be 0.42 kg m^{-2} cm^{-1} or 40-50% more than the value predicted from either one of the two methods individually. The estimated particle-size distribution of the material being eroded consists of 27% gravel, 33% sand, 38% silt, and only 2% clay.

On an annual basis, road surface erosion from Maho-Road is estimated to be close to 50 kg m^{-2}, or four orders of magnitude more than the erosion for undisturbed zero-order hillslopes. This confirms that unpaved roads are a dominant source of sediment on St. John. The event-based models developed in this study can improve the quality of road runoff and sediment yield predictions on St. John. Better predictions may result in the improvement of road drainage design and a reduction on the quantity of sediment reaching the marine environment of St. John.

3.7 References Cited

Anderson B, Potts DF. 1987. Suspended sediment and turbidity following road construction and logging in western Montana. *Water Resources Bulletin* 23: 681-690.

Anderson DM. 1994. Analysis and modeling of erosion hazards and sediment delivery on St. John, U.S. Virgin Islands. US National Park Service Water Resources Division, Technical Report NPS/NRWRD/NRTR-94-34, Fort Collins, Colorado, 153 p.

Anderson DM, MacDonald LH. 1998. Modelling road surface sediment production using a vector geographic information system. *Earth Surface Processes and Landforms* 23: 95-107.

Bilby RE, Sullivan K, Duncan SH. 1989. The generation and fate of road-surface sediment in forested watersheds in southwestern Washington. *Forest Science* 35(2): 453-468.

Bowden MJ, Fischman N, Cook P, Wood J, and Omasta E. 1970. Climate, water balance, and climatic change in the northwest Virgin Islands. Caribbean Research Institute, College of the Virgin Islands, 127 p.

Bren LJ, Leitch CJ. 1985. Hydrologic effects of a stretch of forest road. *Australian Forest Research* 15(2): 183-194.

Calversbert RJ. 1970. Climate of Puerto Rico and the U.S. Virgin Islands. Climatography of the United States No. 60-52, US Dept. of Commerce, 29 p.

CH2M Hill. 1979. A sediment reduction program: Report to the Department of Conservation and Cultural Affairs, Government of the U.S. Virgin Islands, St. Thomas, USVI.

Chow, VT. 1998. Handbook of Applied Hydrology. McGraw-Hill, New York, NY.

Coker RJ, Fahey BD, Payne JJ. 1993. Fine sediment production from truck traffic, Queen Charlotte Forest, Marlborough Sounds, New Zealand. *Journal of Hydrology (N.Z.)* 31(1): 56-64.

Croke J, Mockler S. 2001. Gully initiation and road-to-stream linkage in a forested catchment, southeastern Australia. *Earth Surface Processes and Landforms* 26(2): 205-218.

Dunne T, Leopold L. 1978. Water in Environmental Planning. W.H. Freeman and Company, New York, NY, 818 p.

Fahey BD, Coker RJ. 1992. Sediment production from forest roads in Queen Charlotte Forest and potential impact on marine water quality, Marlborough Sounds, New Zealand. New Zealand *Journal of Marine and Freshwater Research* 26: 187-195.

Flerchinger GN, Watts FJ. 1987. Predicting infiltration parameters for a road sediment model. *Transactions of the ASAE* 30(6): 1700-1705.

Gee GW, Bauder JW. 1986. Particle-size analysis. In: A. Klute (ed.) Methods of Soil Analysis Part 1: Physical and Mineralogical Methods. American Society of Agronomy: 383-411.

Gray DM. 1960. Derivation of hydrographs for small watersheds from measurable physical characteristics. Ph.D. dissertation, Iowa State University of Science and Technology, 208 p.

Grayson RB, Haydon SR, Jayasuriya MDA, Finlayson BL. 1993. Water quality in mountain ash forests- separating the impacts of roads from those of logging operation. *Journal of Hydrology* 150: 459-480.

Gresswell S, Heller D, Swanston DN. 1979. Mass movement response to forest management in the central Oregon Coast Ranges. USDA Forest Service Resource Bulletin PNW-84, Portland, OR, 26 p.

Harden CP. 1992. Incorporating roads and footpaths in watershed-scale hydrologic and soil erosion models. *Physical Geography* 13(4): 368-385.

Helvey JD, Kochenderfer JN. 1990. Soil density and moisture content on two unused forest roads during first 30 months after construction. USDA Forest Service Research Paper NE-629, 6 p.

Henderson FM, Wooding RA. 1964. Overland flow and groundwater flow from a steady rainfall of finite duration. *Journal of Geophysical Research* 69(8): 1531-1540.

Hubbard DK. 1987. A general review of sedimentation as it relates to environmental stress in the Virgin Islands Biosphere Reserve and the eastern Caribbean in general. Biosphere Reserve Report no. 20, Virgin Islands Resource Management Cooperative, St. Thomas, 42 p.

Ice G. 1986. A study of the effectiveness of sediment traps for the collection of sediment from small plot studies. NCASI Technical Bulletin 483, New York, NY, 27 p.

Jones JA, Grant GE. 1996. Peak flow responses to clear-cutting and roads in small and large basins, western Cascades, Oregon. *Water Resources Research* 32(4): 959-974.

Julien PY. 1995. Erosion and Sedimentation. Cambridge University Press, 280 p.

Kahklen KF. 1994. Surface erosion from a forest road, Polk Inlet, Prince of Wales Island, Alaska. M.S. thesis, Oregon State University, Corvallis, OR, 95 p.

La Marche JL, Lettenmaier DP. 2001. Effects of forest roads on flood flows in the Deschutes River, Washington. *Earth Surface Processes and Landforms* 26(2): 115-134.

Luce C. 1990. Analysis of infiltration and overland flow from small plots on forest roads. M.S. thesis, University of Washington, Seattle, WA, 64 p.

Luce CH, Cundy TW. 1992. Modification of the kinematic wave-Phillip infiltration overland flow model. *Water Resources Research* 28(4): 1179-1186.

Luce CH, Cundy TW. 1994. Parameter identification for a runoff model for forest roads. *Water Resources Research* 30(4): 1057-1069.

MacDonald LH, Anderson DM, Dietrich WE. 1997. Paradise threatened: Land use and erosion on St. John, US Virgin Islands. *Environmental Management* 21(6): 851-863.

MacDonald LH, Sampson RW, Anderson DM. 2001. Runoff and road erosion at the plot and road segment scales, St. John, US Virgin Islands. *Earth Surface Processes and Landforms* 26: 251-272.

McCuen RH. 1998. Hydrologic Analysis and Design. Prentice Hall, New Jersey, 814 p.

Megahan WF. 1972. Subsurface flow interception by a logging road in mountains of central Idaho. National Symposium on Watersheds in Transition. American Water Resources Association and Colorado State University, 350-356.

Megahan WF. 1978. Erosion processes on steep granitic road fills in central Idaho. *Soil Science Society of America Journal* 42(2): 350-357.

Megahan WF, Wilson M, Monsen SB. 2001. Sediment production from granitic cutslopes on forest roads in Idaho, USA. *Earth Surface Processes and Landforms* 26(2): 153-164.

Montgomery DR. 1994. Road surface drainage, channel initiation, and slope instability. *Water Resources Research* 30(6): 1925-1932.

Nash JE, Sutcliffe JV. 1970. River flow forecasting through conceptual models, Part 1- A discussion of principles. *Journal of Hydrology* 10: 282-290.

Natural Resources Conservation Service. 1995. Classification and correlation of the soils of the Virgin Islands of the United States-Update. U.S. Department of Agriculture, Hato Rey, Puerto Rico, 18 p.

Ramos-Scharrón, MacDonald LH. 2003. Measuring and modeling the effects of development on sediment production and delivery, St. John , U.S. Virgin Islands. *EOS, Transactions AGU Fall Meeting Supplement 84(46),* Abstract H51F-07: F755-F756.

Rankin DW. 2002. Geology of St. John, U.S. Virgin Islands. U.S. Geological Survey Professional Paper 1631, 36 p.

Rawls WJ, Brakensiek DL, Miller N. 1983. Green-Ampt infiltration parameters from soils data. *Journal of Hydraulic Engineering* 109(1): 62-70.

Reid LM. 1981. Sediment production from gravel-surfaced roads, Clearwater basin, Washington, Publication FRI-UW-8108, University of Washington Fisheries Research Institute, Seattle, WA, 247 p.

Reid LM, Dunne T. 1984. Sediment production from forest road surfaces. *Water Resources Research* 20(11): 1753-1761.

Rice RM, Tilley FB, Datzman PA. 1979. A watershed's response to logging and roads: South Fork of Caspar Creek, California, 1967-1976. U.S. Dept. of Agriculture, Forest Service, Research Paper PSW-146, Berkeley, CA, 12 p.

Sampson RW. 1999. Road runoff and erosion at the plot and road segment scales on St. John, US Virgin Islands. M.S. thesis, Department of Earth Resources, Colorado State University, Fort Collins, CO, 189 p.

Scott HD. 2000. Soil Physics- Agricultural and Environmental Applications. Iowa State University Press, Iowa, 421 p.

Simons DB, Li RM, Shiao LY. 1977. Formation of a road sediment model. Civil Engineering Dept., Engineering Research Center. Colorado State University, Fort Collins, CO, Report CER76-77DBS-RML-LYS50, 107 p.

Simons DB, Li RM, Ward TJ, Shiao LY. 1978. Simple road sediment yield model. USDA Forest Service Report, Fort Collins, CO, Report CER77-78-DBS-RML-TJW-LYS41, 70 p.

Thomas RB, Megahan WF. 1998. Peak flow responses to clear-cutting and roads in small and large basins, western Cascades, Oregon: A second opinion. *Water Resources Research* 34(12): 3393-3403.

Vincent KR. 1979. Runoff and erosion from a logging road in response to snowmelt and rainfall. M.S. thesis, University of California, Berkeley, CA; 60 p.

Wald AR. 1975. The impact of truck traffic and road maintenance on suspended-sediment yield from a 14' standard forest road. MS thesis, University of Washington, Seattle.

Wemple BC, Jones JA, Grant GE. 1996. Channel network extension by logging roads in two basins, western Cascades, Oregon. *Water Resources Bulletin* 32(6): 1195-1207.

Wemple BC, Swanson FJ, Jones JA. 2001. Forest roads and geomorphic process interactions, Cascade Range, Oregon. *Earth Surface Processes and Landforms* 26(2): 191-204.

Woodbury RO, Weaver PL.1987. The vegetation of St. John and Hassel Island, USVI. National Park Service, Southeast Region, Research/Resources Management Report SER-83, Atlanta, GA, 26 p.

Woolhiser DA. 1975. Simulation of unsteady overland flow. In: Unsteady Flow in Open Channels (K Mahmod and V. Yevjevich, Eds), Water Resources Publications, Fort Collins, CO, Vol. 2: 485-508.

Ziegler AD, Giambelluca TW. 1997. Importance of rural roads as source areas for runoff in mountainous areas of northern Thailand. *Journal of Hydrology* 196: 204-229.

Ziegler AD, Sutherland RA, Giambelluca TW. 2000. Partitioning total erosion on unpaved roads into splash and hydraulic components: The roles of interstorm surface preparation and dynamic erodibility. *Water Resources Research* 36(9): 2787-2791.

Ziegler AD, Giambelluca TW, Sutherland RA. 2001a. Erosion prediction on unpaved mountain roads in northern Thailand: validation of dynamic erodibility modelling using KINEROS2. *Hydrological Processes* 15: 337-358.

Ziegler AD, Sutherland RA, Giambelluca TW. 2001b. Interstorm surface preparation and sediment detachment by vehicle traffic on unpaved mountain roads. *Earth Surface Processes and Landforms* 26: 235-250.

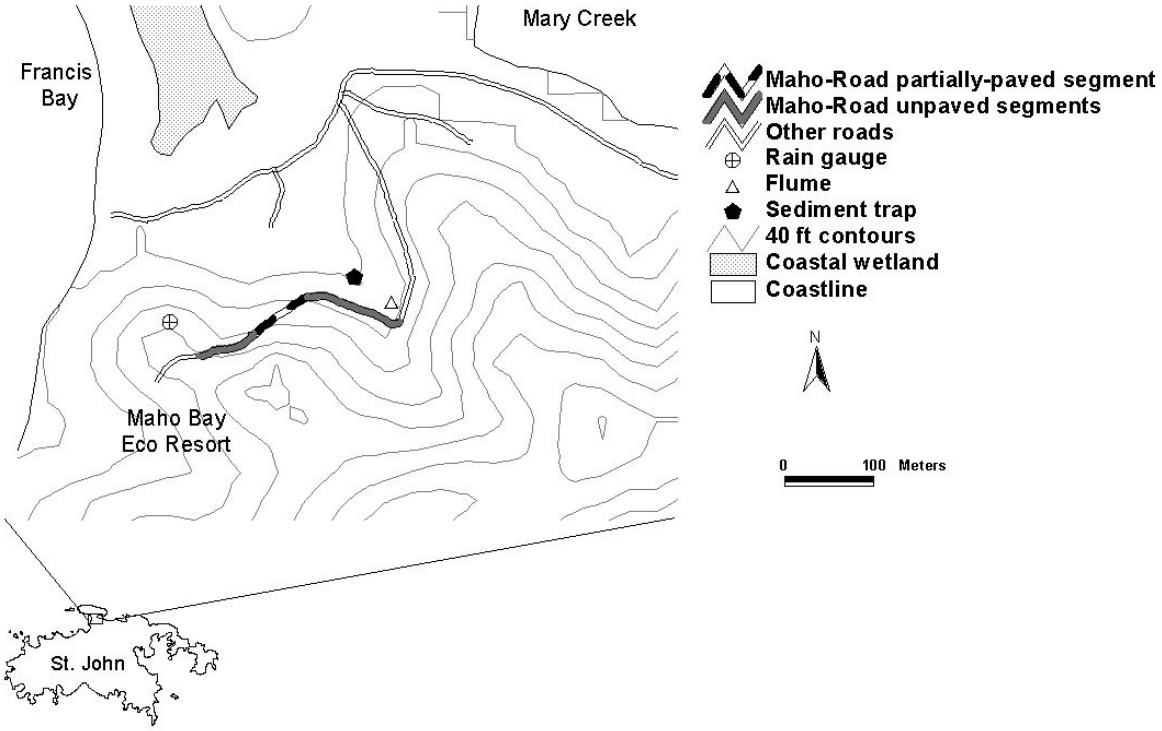

Figure 1. Map of the Maho Bay area showing the road segment that was studied and the location of the rain gauge, cutthroat flume, and sediment trap.

Figure 2a. Picture of the lower sections of Maho-Road.

Figure 2b. Picture of a portable cutthroat flume similar to the one used to measure runoff from Maho-Road.

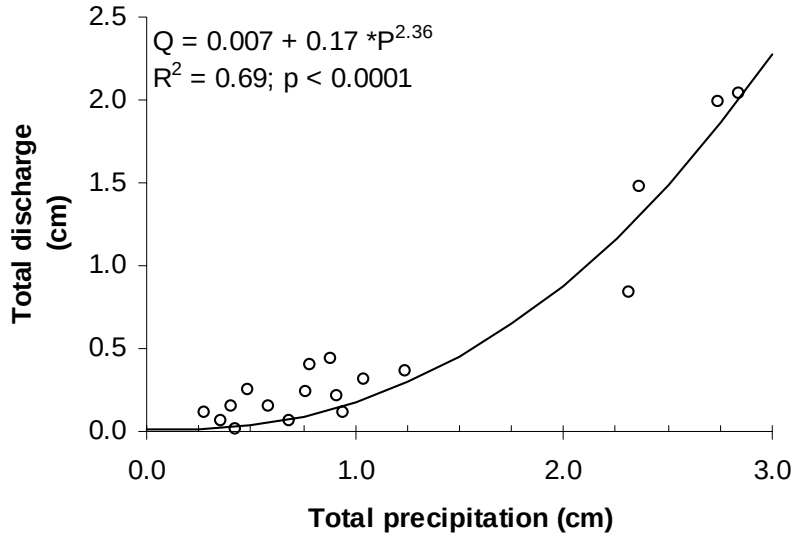

Figure 3. Relationship between precipitation (P) and observed discharge (Q) for the 26 events that produced runoff.

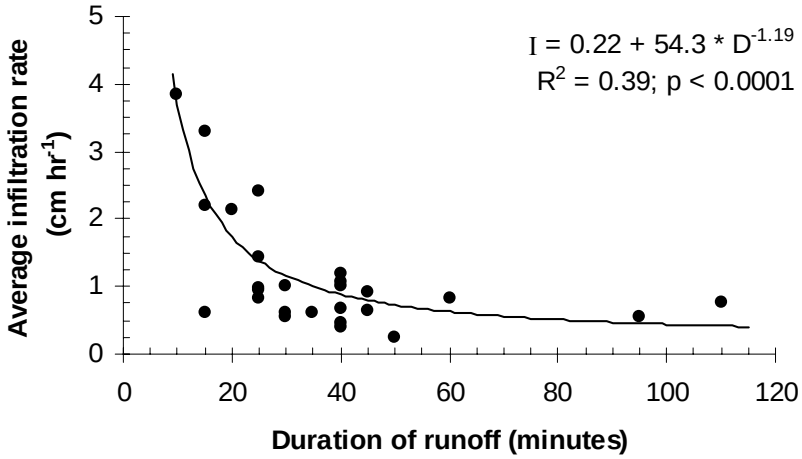

Figure 4. Relationship between duration of runoff (D) and average infiltration rate (I) for the 26 events that produced runoff.

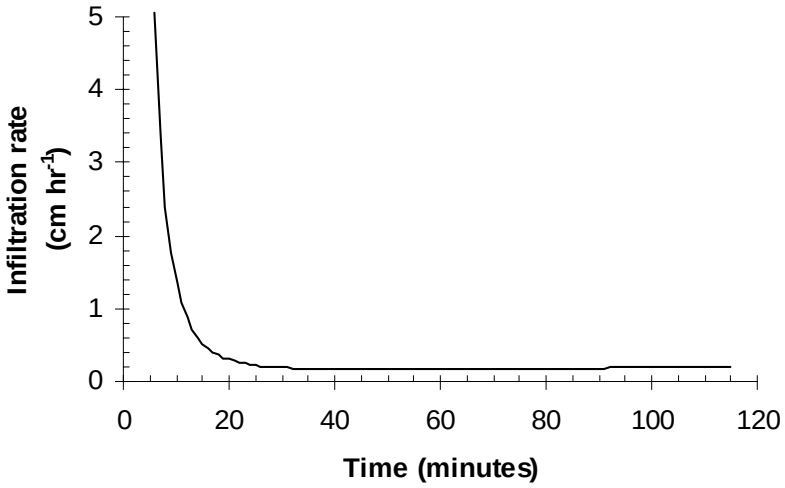

Figure 5. Inferred infiltration curve for Maho-Road.

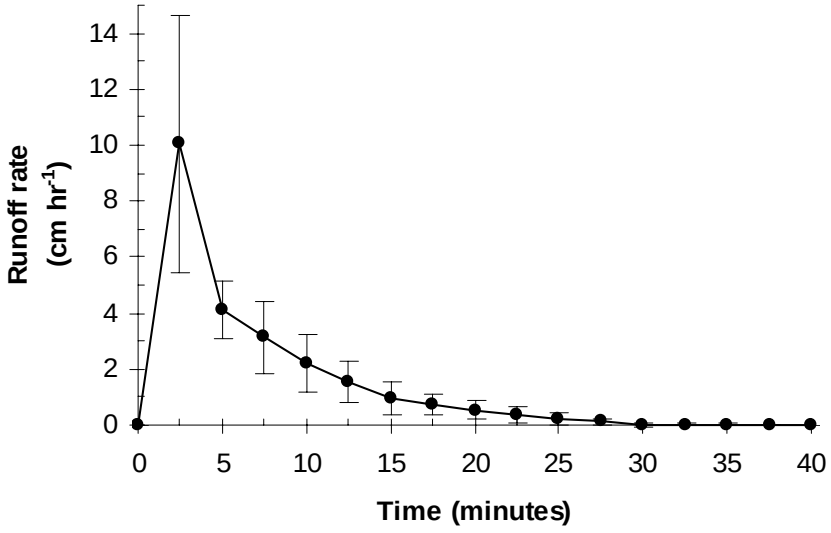

Figure 6. Mean 2.5-minute unit hydrograph from 1.0 cm of excess precipitation for Maho-Road. Bars indicate one standard deviation.

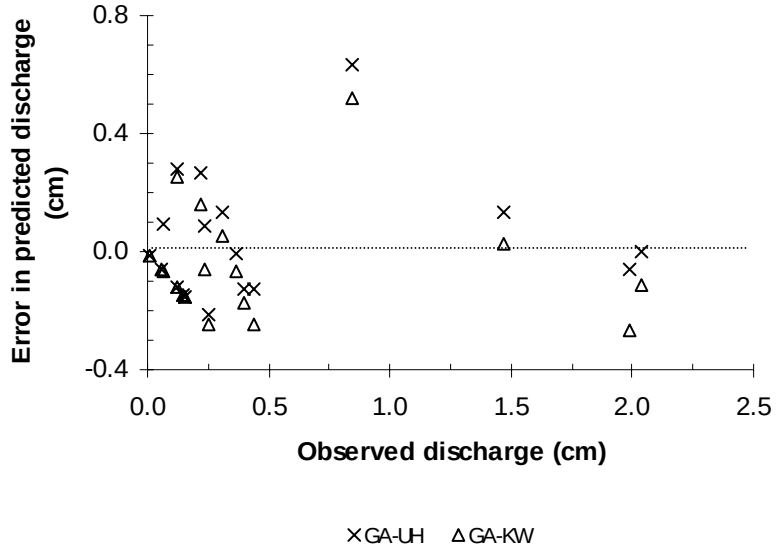

Figure 7. Relationship between total observed discharge and the net error in discharge prediction for 18 event used for model validation.

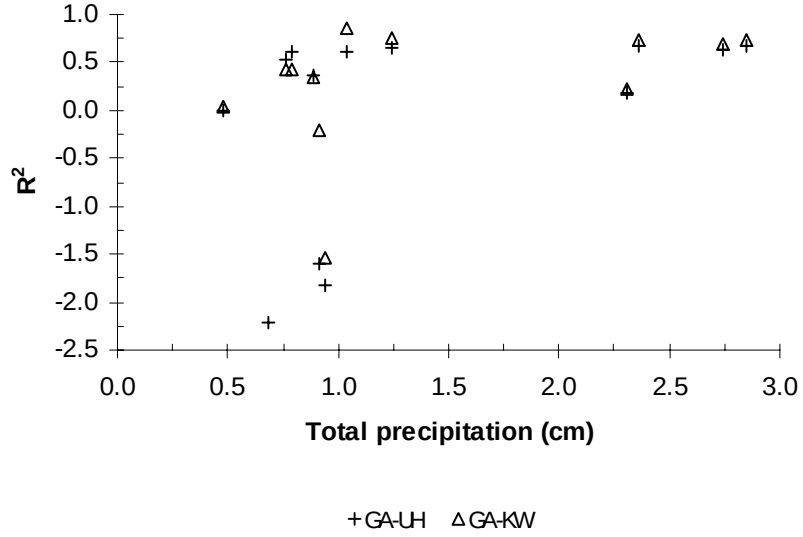

Figure 8. Plot of the coefficient of determination (R^2) between the predicted and observed hydrographs as a function of storm size.

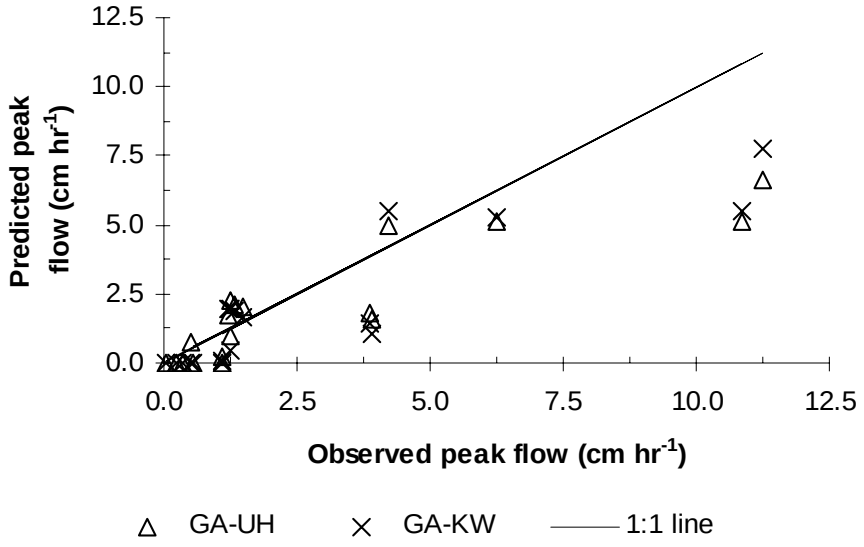

Figure 9. Relationship between measured and predicted peak runoff rates for the 18 storms used for model validation.

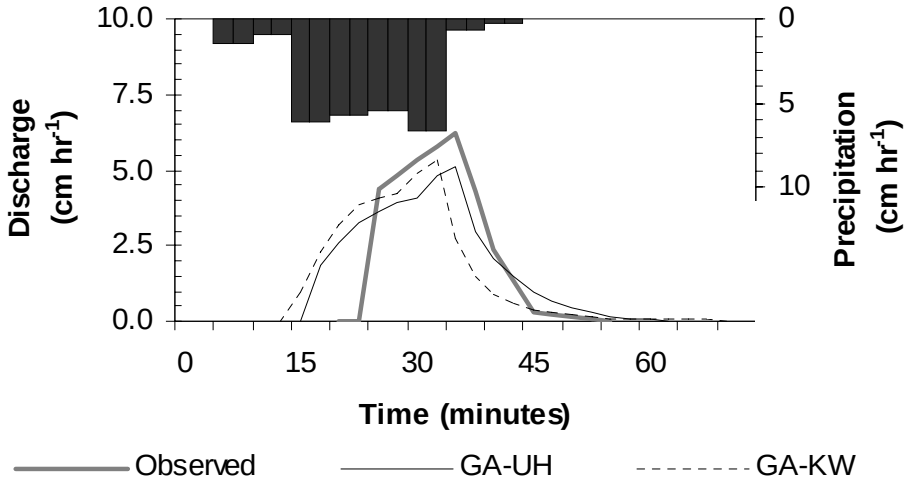

Figure 10a. Hyetograph, observed hydrograph, and simulated hydrograph for the storm on 5 January 2000.

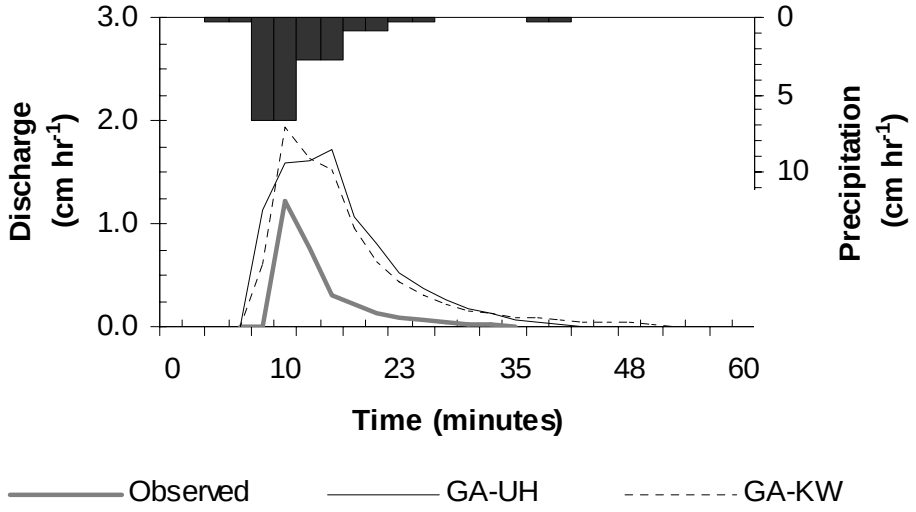

Figure 10b. Hyetograph, observed hydrograph, and simulated hydrograph for the 27 September 1999_c storm.

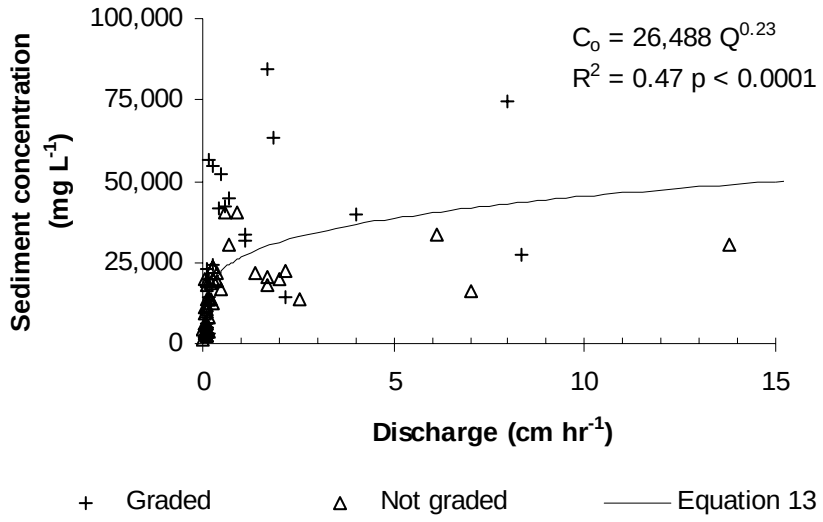

Figure 11. Relationship between suspended sediment concentrations (C_o) and discharge (Q). Maho-Road was graded on 10 September 1999, and the data from 12 September to 25 October 1999 are plotted using a plus sign.

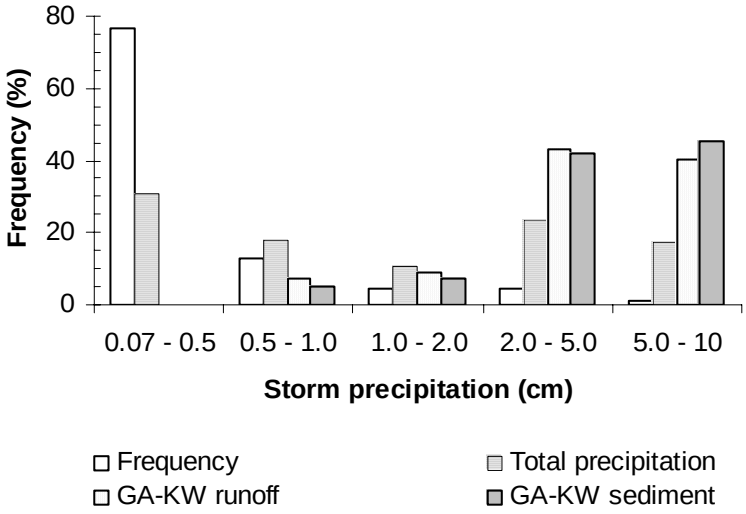

Figure 12. Relative frequency by storm size for 160 storms between 2 September 1999 and 16 May 2000. Percent of the total runoff and sediment yields were calculated with the GA-KW model and equation 13, respectively.

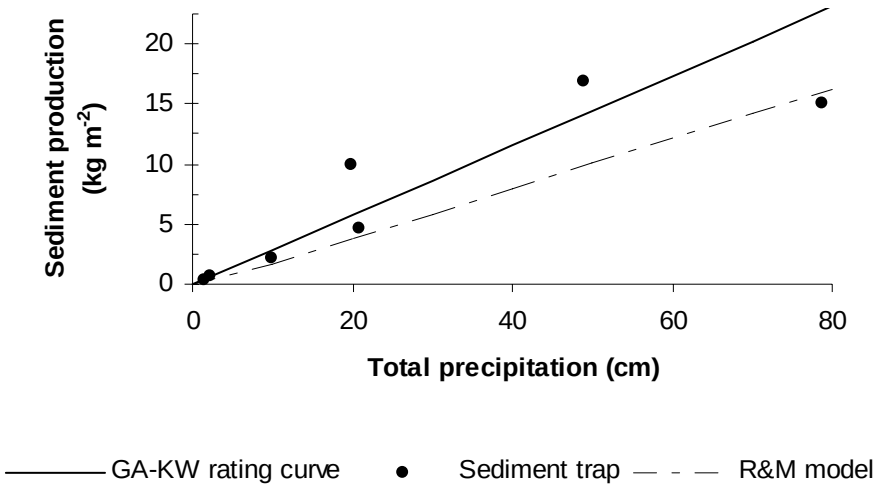

Figure 13. Relationship between total precipitation and sediment production for the GA-KW-sediment rating curve model, the sediment trap from Maho-Road, and the R&M empirical sediment production model.

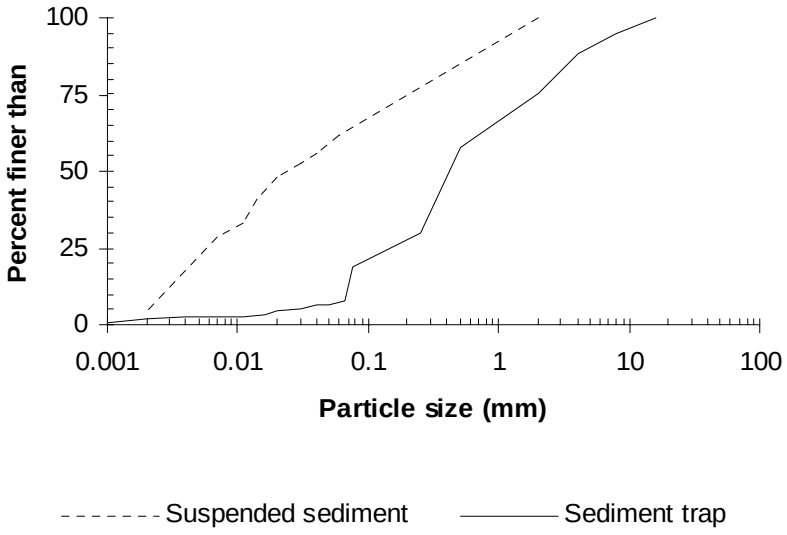

Figure 14. Average particle-size distribution for the suspended sediment samples and the sediment trap data.

Table 1. Summary of previous hydrologic and suspended sediment data for unpaved roads.

Reference	Scale and type of measurements	Runoff coefficient (cm cm^{-1})	Average infiltration (cm hr^{-1})	Hydraulic conductivity (cm hr^{-1})	Sediment concentration (mg L^{-1})	Percentage of sediment by size categories
Bilby et al., 1989	Segment scale (700-3,600 m^2) runoff/sed. yield measurements	--	--	--	70 to 10,000 all traffic intensities	80% clays 20% silt and coarser
Bren & Leitch, 1985	Segment scale (2,100 m^2) runoff measurements	0.04 to 0.80		--	--	--
Coker et al., 1993	Sub-segment scale (35-60 m^2) runoff/sed. yield measurements	0.42 to 0.66	--	--	3,000 to 15,000 no truck traffic 130,000 during truck passes	--
Fahey & Coker, 1992	Sub-segment scale (100 m^2) runoff/sed. yield measurements	--	0.3	--	3,000	85% silts & clays 15% sand & coarser
Grayson et al., 1993	Segment scale (~1,100 m^2) sediment yield measurements	--	--	--	23,000 low use/maint. 35,000-40,000 high use/maint.	66% fines 33% coarse
Harden, 1992	Sub-plot scale (0.02 m^2) infiltration/rainsplash measurements	0.00 to 1.0	0.4 to 3.6	--	520 to 227,000	--
Kahklen, 1994	Road-segment scale (100-250 m^2) runoff/sed. yield measurements	--	0.09	--	0.2 to 118	--
Luce, 1990 Luce & Cundy, 1992	Plot scale (1 m^2) runoff measurements	--	--	0.17 to 0.60	--	--
Luce & Cundy, 1994	Plot scale (1-5 m^2) runoff measurements	--	--	0.21 to 0.50	--	--
Reid, 1981 Reid and Dunne, 1984	Road-segment scale (250-920 m^2) runoff/sed. yield measurements	0.44 to 0.58	0.05	--	400 to 30,000 heavy use 70 to 1,000 temporary use	--
Sampson, 1999 MacDonald et al., 2001	Sub-segment scale (35-60 m^2) runoff/sed. yield measurements	0.04 to 0.13	--	--	5,000 to 50,000	4-40% silts & clays 60-96% sand & coarser
Vincent, 1979	Road-segment scale (110-160 m^2) runoff/sed. yield measurements	0.37 to 0.80	0.02 to 0.05	--	--	--
Wald, 1975	Road-segment scale (400-800 m^2) sediment yield measurements	1.0 (assumed)	--	--	100 low use/maintenance 1,300- high use/maintenance	--
Ziegler & Giambelluca, 1997	Sub-plot scale (< 1 m^2) infiltration measurements	0.02 to 0.88 (from simulations)	--	0.02 to 0.5	--	--
Ziegler et al., 2000	Plot scale (~3 m^2) runoff/sed. yield measurements	0.62 to 0.84	0.62 to 3.7	--	--	--
Ziegler et al., 2001b	Plot scale (~3-5 m^2) runoff/sed. yield measurements	0.60 to 0.86	0.62 to 1.6	--	~25,000- mean for control roads 68,000- mean during truck passes 44,000- mean immediately after grading	--

Table 2. Characteristics of the four sub-segments comprising Maho-Road.

Section Number	Total length (m)	Average width (m)	Average slope ($m\ m^{-1}$)	Comments
1	49	4.4	0.10	Top section, unpaved surface
2	48	4.0	0.26	Partially-paved
3	40	6.0	0.13	Unpaved
4	95	6.3	0.09	Lowermost section, unpaved

Table 3. List of storms with reliable rainfall and runoff data. An asterisk indicates those events used in the development of the unit hydrograph and for model calibration.

Event date	Total precipitation (cm)	Erosivity ($MJ\ cm\ ha^{-1}\ hr^{-1}$)	Max 5-min precipitation intensity ($cm\ hr^{-1}$)	Total discharge (cm)	Peak discharge ($cm\ hr^{-1}$)	Runoff coefficient
6-Sep-99	1.04	5.32	4.27	0.312	1.34	0.30
8-Sep-99	0.91	4.27	4.88	0.200	1.23	0.22
12-Sep-99	0.89	2.29	3.35	0.439	3.91	0.49
27-Sep-99_a	0.94	4.34	6.71	0.119	1.22	0.13
27-Sep-99_b*	0.36	0.65	3.35	0.022	0.16	0.06
27-Sep-99_c*	0.61	1.68	3.36	0.060	0.64	0.10
5-Oct-99*	0.94	4.97	7.92	0.144	1.77	0.15
12-Oct-99	0.58	1.10	2.44	0.140	0.24	0.24
13-Oct-99*	0.48	1.16	3.96	0.072	0.40	0.15
20-Oct-99	0.79	2.84	3.96	0.480	3.86	0.61
23-Oct-99	2.84	38.6	12.80	2.16	11.2	0.76
25-Oct-99	0.48	0.91	2.74	0.240	1.08	0.50
30-Oct-99	2.31	23.3	7.92	0.910	4.22	0.39
6-Nov-99	0.41	0.60	1.83	0.148	0.56	0.36
10-Nov-99	1.24	3.55	4.57	0.360	1.50	0.29
11-Nov-99	2.74	22.5	7.62	1.93	12.0	0.70
13-Nov-99	0.28	0.35	2.44	0.130	1.09	0.46
14-Nov-99	0.69	1.29	2.13	0.050	0.56	0.07
16-Nov-99	0.76	1.95	2.44	0.260	1.34	0.34
4-Jan-99*	0.41	0.77	2.40	0.013	0.05	0.03
5-Jan-00	2.36	21.6	6.71	1.36	6.25	0.58
29-Jan-00*	0.61	1.20	3.36	0.016	0.10	0.03
20-Apr-00	0.43	0.50	2.44	0.078	0.05	0.18
22-Apr-00*	0.71	1.82	3.66	0.027	0.16	0.04
29-Apr-00*	0.53	1.49	4.88	0.045	0.50	0.08
2-May-00	0.36	0.25	2.74	0.060	0.33	0.17

Table 4. Range of parameter values considered in model calibration and the final calibrated values selected for the GA-UH and GA-KW models, respectively. Wet conditions refer to events with 6-hr antecedent precipitation greater than zero. NA indicates not applicable.

Parameter	**Range of possible values**	**Unit hydrograph model**	**Kinematic wave model**
Mean K_s (cm hr^{-1})	0.12 - 0.22	0.20	NA
K_s unpaved sections (cm hr^{-1})	0.15 - 0.23	NA	0.23
K_s partially-paved section (cm hr^{-1})	0.00 - 0.22	NA	0.04
Max infiltration rate (cm hr^{-1})	0 - ∞	4.0	4.0
h_f (cm)	2.0 - 8.0	5.4	6.4
$\theta_{saturated}$ (cm^3 cm^{-3})	0.25 - 0.60	0.4	0.4
$\theta_{initial\text{-}dry\ conditions}$ (cm^3 cm^{-3})	0.00 - θ_{sat}	0.00	0.00
$\theta_{initial\text{-}wet\ conditions}$ (cm^3 cm^{-3})	0.00 - θ_{sat}	0.18	0.11
Manning's n, unpaved sections (s $m^{-1/3}$)	0.010 - 0.030	NA	0.010
Manning's n, paved section (s $m^{-1/3}$)	0.010 - 0.013	NA	0.010
β	0 - 1	NA	0.6

Table 5. Summary of model validation results. NA indicates not applicable.

Event	OBSERVED			GA-UH MODEL						GA-KW MODEL					
	Runoff (cm)	Runoff coefficient (cm cm^{-1})	Peak flow (cm hr^{-1})	Predicted runoff (cm)	Error in runoff (cm)	Runoff coefficient (cm cm^{-1})	Peak flow (cm hr^{-1})	Error in peak flow (cm hr^{-1})	R^2	Predicted runoff (cm)	Error in runoff (cm)	Runoff coefficient (cm cm^{-1})	Peak flow (cm hr^{-1})	Error in peak flow (cm hr^{-1})	R^2
6-Sep-99	0.31	0.30	1.34	0.45	0.13	0.43	2.11	0.77	0.61	0.37	0.05	0.35	1.89	0.55	0.86
8-Sep-99	0.22	0.24	1.23	0.48	0.27	0.53	2.26	1.03	-1.60	0.38	0.16	0.41	1.97	0.74	-0.21
12-Sep_b-99	0.44	0.49	3.91	0.31	0.13	0.35	1.57	2.34	0.36	0.20	0.24	0.24	1.09	2.82	0.35
27-Sep_c-99	0.12	0.13	1.22	0.40	0.28	0.42	1.71	0.49	-1.83	0.37	0.25	0.40	1.94	0.72	-1.53
12-Oct-99	0.15	0.26	0.24	0.00	0.15	0.00	0.00	0.24	n/a	0.00	0.15	0.00	0.00	0.24	n/a
20-Oct-99	0.40	0.51	3.86	0.27	0.13	0.35	1.83	2.03	0.61	0.23	0.17	0.29	1.44	2.42	0.42
23-Oct-99	2.04	0.72	11.24	2.04	0.00	0.72	6.66	4.58	0.67	1.92	0.11	0.68	7.76	3.48	0.73
25-Oct-99	0.25	0.52	1.08	0.03	0.22	0.07	0.25	0.83	0.01	0.00	0.25	0.01	0.07	1.01	0.03
30-Oct-99	0.84	0.36	4.22	1.47	0.63	0.64	4.98	0.76	0.18	1.36	0.52	0.59	5.48	1.26	0.23
6-Nov-99	0.15	0.36	0.56	0.00	0.15	0.00	0.00	0.56	n/a	0.00	0.15	0.00	0.00	0.56	n/a
10-Nov-99	0.36	0.29	1.50	0.36	0.01	0.29	2.02	0.52	0.65	0.30	0.06	0.26	1.63	0.13	0.75
11-Nov-99	1.99	0.72	10.86	1.93	0.06	0.70	5.08	5.78	0.62	1.72	0.27	0.63	5.51	5.35	0.70
13-Nov-99	0.12	0.42	1.09	0.00	0.12	0.00	0.00	1.09	n/a	0.00	0.12	0.00	0.00	1.09	n/a
14-Nov-99	0.07	0.10	0.52	0.16	0.10	0.24	0.72	0.20	-2.21	0.00	0.07	0.00	0.00	0.52	n/a
16-Nov-99	0.24	0.24	1.25	0.32	0.08	0.35	0.98	0.27	0.53	0.17	0.06	0.18	0.43	0.82	0.43
5-Jan-00	1.47	0.62	6.25	1.60	0.13	0.68	5.11	1.14	0.67	1.49	0.02	0.63	5.30	0.95	0.74
20-Apr-00	0.01	0.03	0.05	0.00	0.01	0.00	0.00	0.05	n/a	0.00	0.01	0.00	0.00	0.05	n/a
2-May-00	0.06	0.17	0.33	0.00	0.06	0.00	0.00	0.33	n/a	0.00	0.06	0.00	0.00	0.33	n/a
Sum	9.23			9.82	2.65					8.51	2.74				
Mean	0.51	0.36		0.55	0.15	0.32		1.28	-0.06	0.47	0.15	0.26		1.28	0.29
Std. Dev.	0.64	0.21		0.70	0.14	0.26		1.55	1.1	0.66	0.12	0.25		1.38	0.66